Incipient Subduction and Slip Partitioning at High Obliquity: the Haida Gwaii Plate Boundary

S. J. Oliva[1,2], M. G. Bostock[2], A. J. Schaeffer[3], E. Nissen[1], R. Merrill[2], A. Hughes[2], S. W. Roecker[4], M. R. Nedimovic[5], E. Roland[6], L. L. Worthington[7], M. A. L. Walton[8], A. Gase[6]

[1]School of Earth and Ocean Sciences, University of Victoria, Victoria, BC, Canada

[2]Department of Earth, Ocean and Atmospheric Sciences, University of British Columbia, Vancouver, BC, Canada

[3]Geological Survey of Canada, Pacific Division, Natural Resources Canada, Sidney, BC, Canada

[4]Earth and Environmental Sciences, Rensselaer Polytechnic Institute, Troy, NY, USA

[5]Department of Earth Sciences, Dalhousie University, Halifax, NS, Canada

[6]Geology Department, Western Washington University, WA, USA

[7]Department of Earth and Planetary Sciences, University of New Mexico, NM, USA

[8]Ocean Sciences Division, US Naval Research Laboratory, Stennis Space Center, MS, USA

Key Points:

- Seismicity off Moresby Island is distributed along multiple segments slightly off of the Queen Charlotte fault trace
- Aftershocks at intersection of Queen Charlotte Fault with the 2012 Mw 7.8 thrust plane reflect residual stress at slip partitioning juncture
- Previously undocumented deep seismicity beneath Haida Gwaii is consistent with an underthrusting Pacific Plate

Corresponding author: S. J. Oliva, `soliva@uvic.ca`

Abstract

Plate motion obliquity along the dominantly transform Queen Charlotte plate boundary (QCPB) peaks offshore Haida Gwaii. To investigate the effects of obliquity on plate boundary deformation, we analyze continuous seismic waveforms from temporary and permanent stations from 1998—2020 to generate a catalog of $\sim$50,000 earthquakes across Haida Gwaii. We use an automated technique based on auto-regressive phase detection and onset estimation to obtain the initial seismic catalog, integrate existing catalogs, invert for 3D velocity structure using data from the best constrained period, and relocate the entire catalog using the new 3D velocity model. We investigate the seismically active sections of the transcurrent Queen Charlotte fault (QCF), noting that little seismicity locates directly along its bathymetrically defined trace. Instead, seismicity illuminates a complex system of segmented structures with variable geometries along strike. Other clusters highlight active shallow faults within the highly deformed Queen Charlotte terrace. Few aftershocks appear on the thrust plane of the 2012 M_w 7.8 Haida Gwaii earthquake except near its inferred intersection with the QCF at 15–20 km depths, suggesting elevated residual stress at the juncture of slip-partitioning. Deep crustal seismicity (up to $\sim$20 km depths) beneath central Haida Gwaii aligned parallel to the strike of the thrust plane may represent landward underthrusting of the Pacific plate. Our results examine possible coseismic strike-slip rupture on the QCF during the 2012 earthquake and add support to the thesis that highly oblique transform boundaries are viable settings for subduction initiation.

Plain Language Summary

We investigated the complex tectonics offshore Haida Gwaii, western Canada, where the Pacific and North American plates slide past one another obliquely. By compiling and analyzing the most comprehensive earthquake catalog in the area, spanning 1998–2020, we present the most detailed report to date of the earthquake-producing structures in the region, including previously unidentified and highly segmented faults. Clusters of seismicity illuminate (1) a highly deformed terrace of elevated seafloor west of Haida Gwaii, (2) a complex and segmented fault system adjacent to the previously-mapped surface trace of the main Queen Charlotte strike-slip fault, and (3) the inferred fault intersection at depth between the subvertical Queen Charlotte fault (which hosted the 1949 magnitude 8.1 earthquake) and the shallowly dipping Haida Gwaii thrust (which hosted the
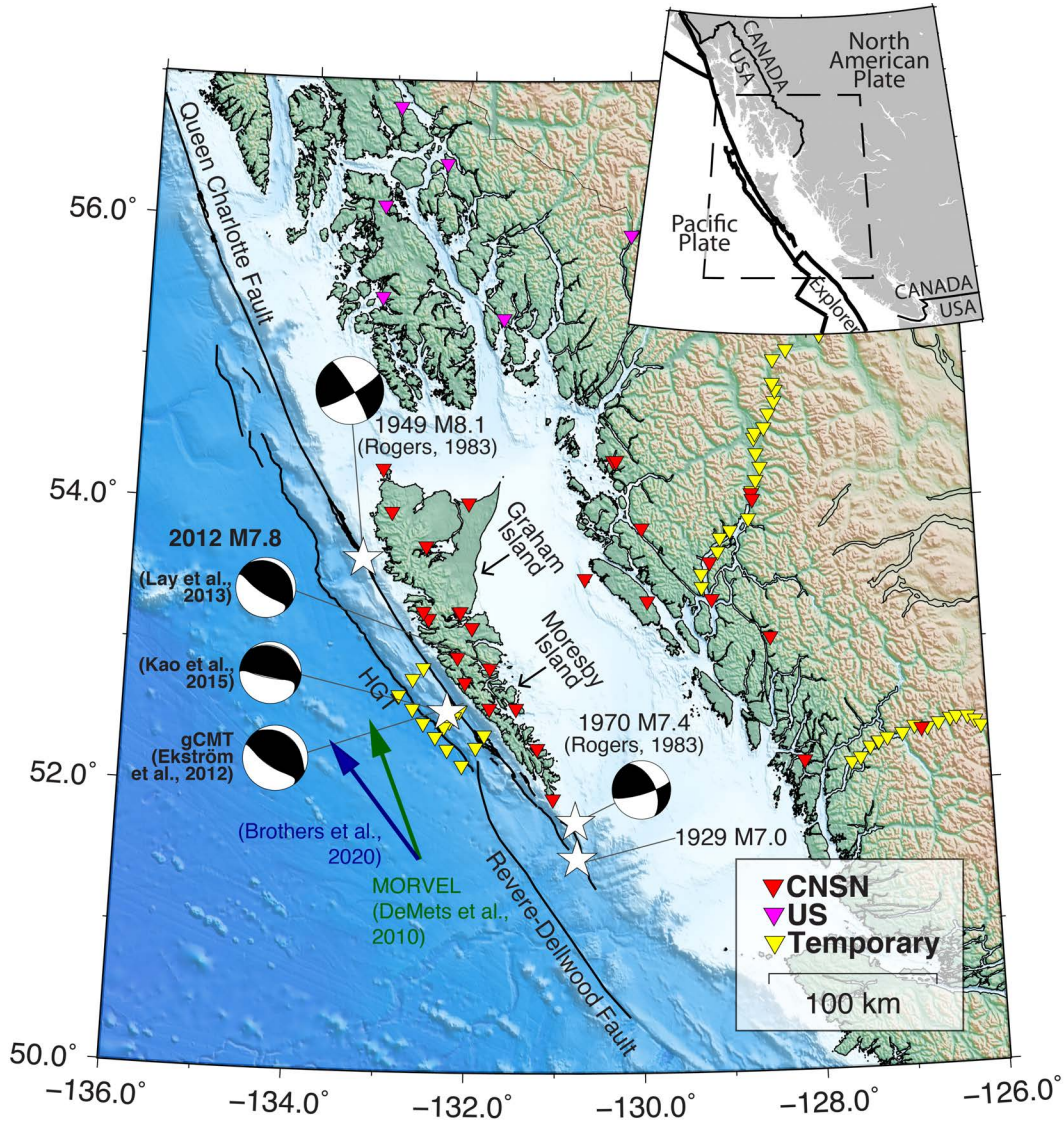
2012 magnitude 7.8 earthquake). We also speculate that the 2012 earthquake may also have involved some motion on the Queen Charlotte fault. These results contribute to better constraints on regional tectonics and hazards, and provide insights into the mechanisms of subduction initiation.

1 Introduction

Subduction initiation is an important element of plate tectonics. As a transient process followed by a protracted period of plate removal, alteration and destruction, limited localities exist for field study in the present day. Recent reviews have highlighted the importance of transform settings in subduction initiation (Stern & Gerya, 2018; Lallemand & Arcay, 2021), in which the transition is supported by changes in plate kinematics and a young compliant oceanic plate. The Queen Charlotte plate boundary (QCPB) at Haida Gwaii exhibits both these attributes (e.g., Hyndman, 2015) and represents a high-obliquity endmember whose characterization promises important insights into the mechanics of subduction initiation.
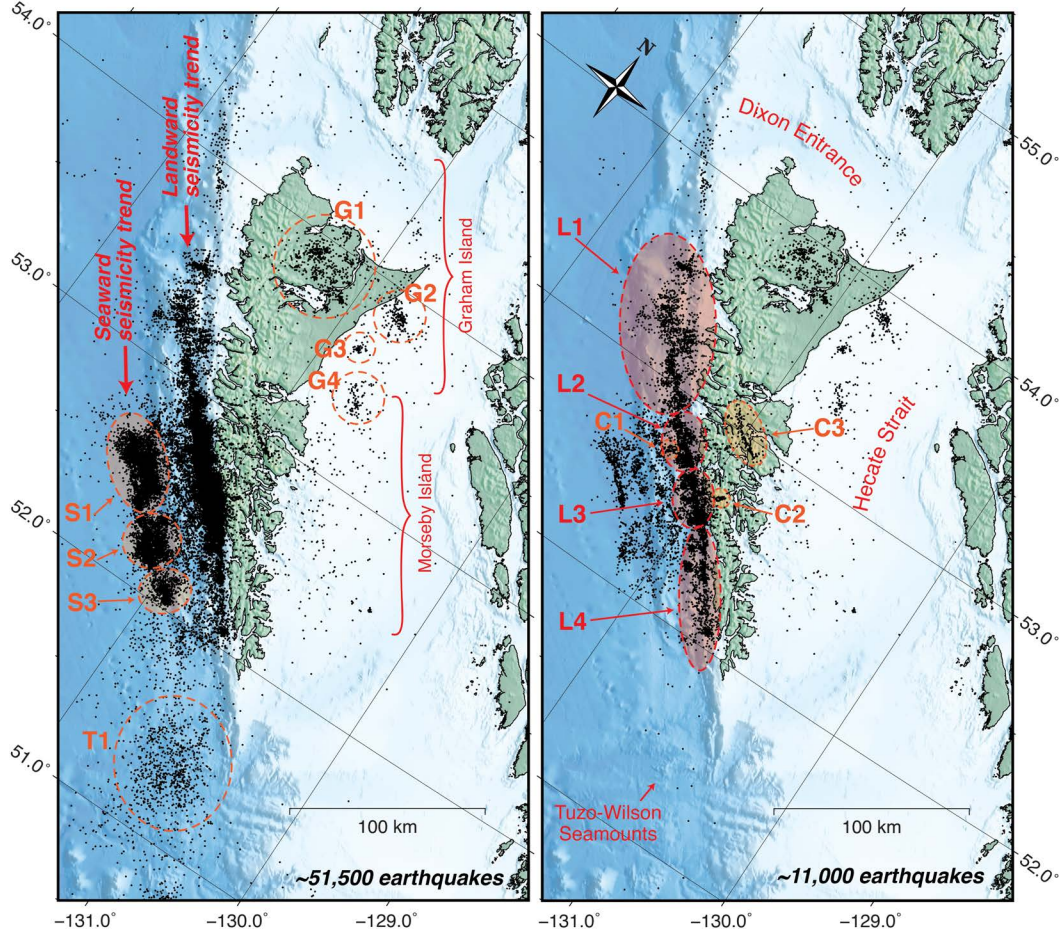
The QCPB forms the dominantly transform margin between the Pacific and North American plates from offshore Haida Gwaii through southeastern Alaska (Fig. 1). The main plate boundary fault is the 850 km-long right-lateral Queen Charlotte Fault (QCF), which slips at 53 mm/yr (Brothers et al., 2020; DeMets et al., 2010; DeMets & Merkouriev, 2016), making it one of the fastest moving strike-slip faults globally. This offshore fault merges northward into the onshore right-lateral Fairweather fault. To the south, it links to the nominal Queen Charlotte triple junction of the Explorer, Pacific, and North American plates, through its overlap with the northernmost extent of the right-lateral Revere-Dellwood fault near 52°N (Riddihough et al., 1980; Rohr, 2015) (Fig. 1).

Along the southern QCPB offshore Haida Gwaii, the orientation of Pacific-North American plate motions with respect to mapped fault geometries introduces a component of shortening (Fig. 1). Estimates of plate motion vectors vary between 5° to 20° clockwise from the QCF strike. Tréhu et al. (2015) reported the angle to be >15° based on the Mid-Ocean Ridge Velocity (MORVEL) global plate motion model (DeMets et al., 2010). Rohr et al. (2000) amended a previous estimate of ∼26° to 20° clockwise from the QCF strike upon later revision of their QCF trace (Rohr, 2015). An updated global plate reconstruction by DeMets and Merkouriev (2016) produced a plate motion vector
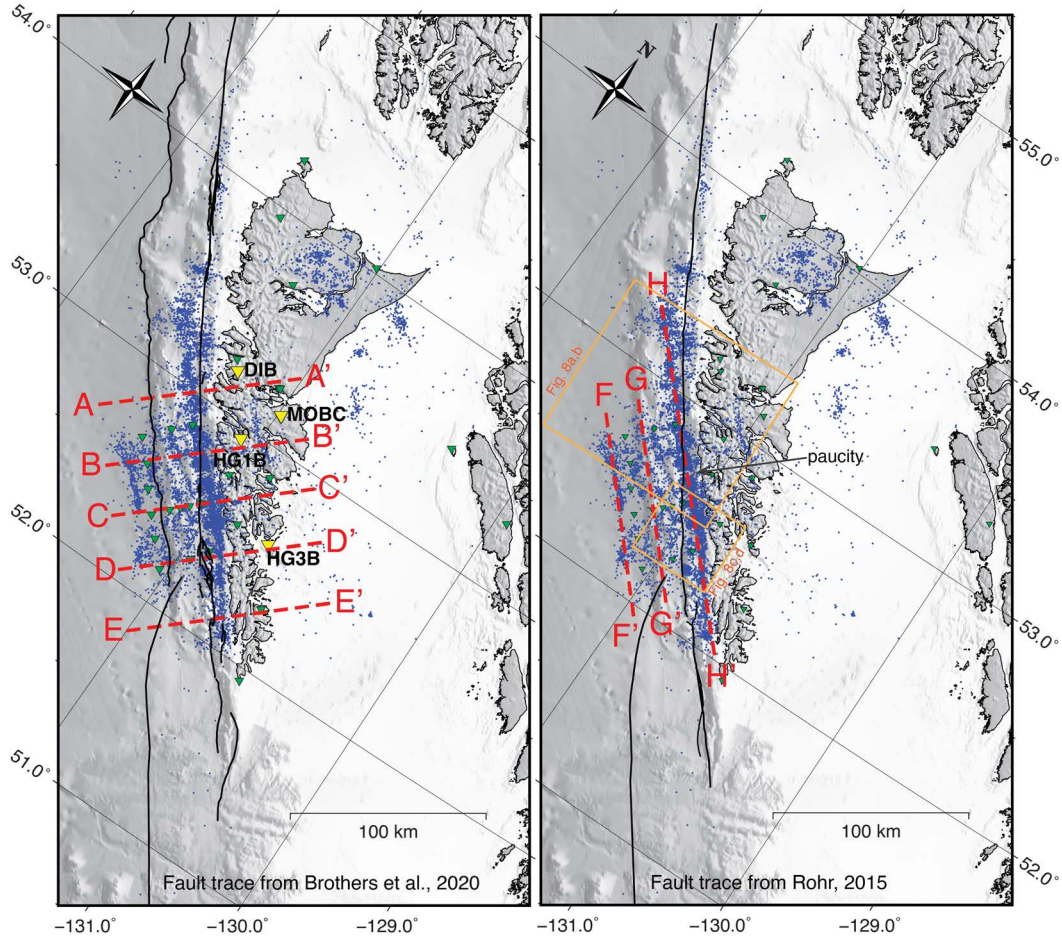
Figure 1. Four of Canada's largest instrumentally-recorded earthquakes (M≥7, white stars) have occurred along the Queen Charlotte Plate Boundary (QCPB). Focal mechanisms for the three most recent of these are plotted, including three solutions for the 2012 M_w 7.8 Haida Gwaii earthquake (Kao et al., 2015; Lay et al., 2013; Ekström et al., 2012; Rogers, 1983). Seismic stations (inverted triangles) used in this study are from the Canadian National Seismograph Network (CNSN, red), US network (magenta), and temporary deployments (yellow). Mapped fault traces are from Brothers et al. (2020). HGT=Haida Gwaii Thrust fault. Upper right inset shows tectonic context. Green and blue arrows show Pacific plate motion from DeMets et al. (2010) and Brothers et al. (2020), respectively.

Figure 2. On the full ∼51,500 relocated earthquake catalog (left), we can clearly identify the subparallel seaward and landward seismicity trends. The ∼11,000 subset (right) better shows the seismicity patterns within the landward seismicity trend, labeled as clusters L1 through L4. Clusters C1–C3 are secondary seismicity patterns of interest. Graham (Haida: *X̲aayda̲ga Gwaay.yaay lina̲gwaay in X̲ayda Kil*) and Moresby (Haida: *T'aaxwii X̲aayda̲ga Gwaay.yaay lina̲gwaay*) Islands are the two main islands of Haida Gwaii. Fig. 3 shows interpreted locations of the principal QCF trace which are not plotted here so as not to obscure seismicity or bathymetric detail.

Figure 3. Map of the ∼11,000 earthquake subset (blue) with the across-fault (left) and along-strike (right) transects shown in Figs. 5 and 6, respectively. Yellow triangles in the left panel are stations for which receiver functions are plotted on Fig. 5. Green triangles are other stations. The mapped QCF traces of Brothers et al. (2020) and Rohr (2015) are shown in the left and right panels, respectively. Orange boxes outline Fig. 8a–b and c–d.

85 of 21° from the QCF strike, a departure of 1° from MORVEL (DeMets et al., 2010). Brothers

86 et al. (2020) reconstructed the QCF motion based on tectonic geomorphology and remapped

87 the QCF trace to lie closer to shore between 52–52.4°N compared to Rohr (2015) (Fig. 3).

88 On the basis of bathymetric signature and a near small-circle trajectory on more northerly

89 portions of the QCF, Brothers et al. (2020) further argued that global plate motion mod-

90 els significantly overestimate convergence along southern Haida Gwaii and that the dif-

91 ference between the plate motion vector and the QCF strike is only 5.6°.

92   In addition to the degree of plate-motion obliquity, debate has also centered on whether

93   convergence is accommodated by underthrusting of the Pacific plate beneath the North

94   American plate (DeMets & Merkouriev, 2016; Hyndman, 2015; Wang et al., 2015) or only

95   by internal deformation of the Pacific and North America plates, involving lithospheric

96   thickening and shortening (Brothers et al., 2020; Rohr et al., 2000). Receiver function

97   studies report evidence for a 10–17 km-thick low velocity zone dipping 15–30° for at least

98   50 km landward of the QCF beneath Haida Gwaii, interpreted as the top of the under-

99   thrusting Pacific plate (Bustin et al., 2007; Gosselin et al., 2015; Smith et al., 2003). Sea-

100   ward and subparallel to the QCF, the 30 km-wide submarine Queen Charlotte terrace

101   (QCT), composed of faulted and folded sediments and possibly oceanic crust (Riedel et

102   al., 2021; Rohr et al., 2000; Tréhu et al., 2015), has been likened to an accretionary prism,

103   thus pointing to possible subduction initiation (Hyndman, 2015). Within a subduction

104   initiation configuration, the terrace would define a forearc sliver, a feature observed in

105   various other oblique convergent settings around the world (e.g., Cassidy et al., 2014;

106   Jarrard, 1986). In this study, we use the terminology "Haida Gwaii thrust fault (HGT)"

107   (Hyndman, 2015) to refer to the fault or fault system beneath the terrace that hosted

108   the 2012 M_w 7.8 thrust event (e.g., Lay et al., 2013; Nykolaishen et al., 2015)—the downdip

109   extent of which remains debated. While Cassidy et al. (2014) have taken the 2012 earth-

110   quake as the strongest evidence for an underthrusting oceanic plate, the lower conver-

111   gence component of Brothers et al. (2020) led the latter to question the degree of un-

112   derthrusting. In the absence of a through-going slab, the terrace would represent oceanic

113   crust deformed and thickened from compression (Dehler & Clowes, 1988; Rohr et al., 2000)

114   with the QCF as the backstop of deformation concentrated along the edge of a hot and

115   weak oceanic plate (Brothers et al., 2020).

116   The M_w 7.8 Haida Gwaii earthquake occurred on October 28, 2012 (October 27,

117   local time) along the QCPB offshore Moresby Island (Fig. 2), which provided evidence

118   that the Haida Gwaii margin represents a stage of localized subduction initiation (in the

119   parlance of Lallemand and Arcay (2021)), as well as reignited debate on the extent of

120   underthrusting beneath Haida Gwaii. The earthquake produced a local tsunami and had

121   a predominantly thrust mechanism, with the preferred fault plane dipping shallowly NNE

122   and striking 311° (Kao et al., 2015), 317° (Lay et al., 2013), or 318° (the global Centroid

123   Moment Tensor or gCMT, Ekström et al., 2012) (Fig. 1). There were very few thrust

124   aftershocks (Kao et al., 2015; Lay et al., 2013), and most of the larger aftershocks were

normal-faulting events located west of the QCT, interpreted as evidence for bending stresses on the Pacific plate (Kao et al., 2015) and consistent with modelled Coulomb stress changes (Lay et al., 2013). Whereas back-projected high-frequency seismic radiation might suggest energy release farther downdip beneath Moresby Island (Lay et al., 2013), Global Navigation Satellite System (GNSS) coseismic displacements suggest that rupture probably does not extend farther landward from the coast (Nykolaishen et al., 2015). However, the GNSS-derived slip model resolution is limited during the 2012 mainshock as there was only one continuous GNSS site in operation, located 80 km to the north-northeast. GNSS-based models of postseismic deformation reveal up to 30 cm of thrust afterslip downdip of the coseismic rupture within 7 years of the mainshock (Tian et al., 2021), along with between 1.5 and 9.0 cm of right-lateral afterslip on the vertical QCF in the first year (Guns et al., 2021). These models are consistent with repeating earthquakes which suggest short-lived postseismic motion on the QCF ($\sim$2 months) and longer on the HGT (at least 3 years) (Hayward & Bostock, 2017).

The QCPB appears to reside primarily if not entirely offshore, resulting in generally poor azimuthal seismic coverage since regional land stations are all located east of the plate boundary. Fortunately in December 2012, in response to the M_w 7.8 earthquake, the Geological Survey of Canada deployed 14 ocean-bottom seismometers (OBS) offshore Haida Gwaii to record aftershocks (Fig. 1) (Riedel et al., 2021), providing about two weeks of improved data coverage to constrain the plate boundary and the offshore seismicity. Moreover, an additional 7 short-period land stations were deployed in the first week of November 2012; one was operational for only a month (MOBC2), three recorded data until May 2013 (HGPB/HGSB, TSUB, STJA), and the other three had broadband instruments swapped in after the first week (Gosselin et al., 2015). Of the broadband stations, HG3B continued running until 2014, HG1B remains in operation to the current date, and HG4B was reoccupied as JEDB and is active to this day. Capitalizing on these ten years of improved seismic instrumentation, as well as seismic data from twenty years prior, our study aims to characterize the seismicity along the southern QCPB offshore Haida Gwaii in space and time. We use the new earthquake catalog to investigate the configuration of and slip partitioning across the plate margin, including underthrusting along the HGT, the transform QCF, and the potential role of the QCT as a "forearc" sliver.

2 Data and Methods

To augment the existing Geological Survey of Canada earthquake catalog, we employed the `REST` (Regressive ESTimator) automated catalog generation package written and maintained by S. W. Roecker. Details of this package are discussed in Comte et al. (2019) and Lanza et al. (2019). To summarize, `REST` combines the autoregessive approach of Pisarenko et al. (1987) and Kushnir et al. (1990) for P and S wave phase detection and onset estimation with the windowing strategies of Rawles and Thurber (2015) and hypocenter location algorithms of Roecker et al. (2006), to iteratively refine arrival times and reject false positives.

To create our new catalog, we used all available continuous seismic waveform data from 1998 to 2020 for the region between longitudes 136°W and 126°W and latitudes 50°N and 57°N, including the two transects of the Batholiths project (2005-2006) across the Coast Mountains (Calkins et al., 2010) and the Geological Survey of Canada's OBS deployment in 2012 (Riedel et al., 2021). Our automated catalog included 47,628 events with at least 4 paired P and S picks. Within the same time period and region, the Canadian National Seismographic Network (CNSN) reported 14,716 earthquakes. We also included an additional 643 events registered by the CNSN between 1992 to 1998, as well as the Alaska Network (AK) catalog which reported 355 earthquakes in the region over the period 1998–2020. We combined the three catalogs (REST, CNSN, AK), merging events with origin times within 5 s and located within 0.5° latitude and longitude. Automated REST picks were overwritten with CNSN and AK event picks (which are generally screened by analysts), when available for the same event.

The combined catalog with merged picks (53,933 events with at least 4 paired P and S picks) was relocated with `Hypoinverse v.1.4` using the program's multimodel feature. An oceanic velocity model based on a 1983 seismic refraction project west of Haida Gwaii in the Pacific (Dehler & Clowes, 1988) was assigned west of the QCF trace of Rohr (2015), and a continental model based on a 1988 seismic refraction-reflection survey east of Haida Gwaii in the Hecate Strait (Line 6 Spence & Asudeh, 1993) was assigned to the east. We assumed an initial Vp/Vs ratio of 1.76, determined from a Wadati plot of the initial catalog. Given the large number of earthquakes, we sought to better define the associated velocity structure using a small but densely sampled subset of the catalog before relocating the remaining events.

189   The two weeks with continuous OBS data in December 2012—which, in combina-

190   tion with high aftershock rates, produced the best multi-station coverage of the region—

191   were used to build the 3D velocity model. First we constructed a starting 3D velocity

192   model from the aforementioned 1D oceanic and continental velocity models (Dehler &

193   Clowes, 1988; Spence & Asudeh, 1993), stitched together and smoothed over 30 km across

194   the QCF trace (Rohr, 2015). The model domain is 300 km × 400 km × 200 km, cen-

195   tered at 53°N 132.6°W, rotated 35° counterclockwise, with a nodal spacing of 5 km along

196   the horizontal and 3 km along the vertical. We performed `Hypoinverse` and `hypoDD` (Waldhauser

197   & Ellsworth, 2000) double-difference relocations separately for the oceanic and the con-

198   tinental sides, then used those relocations as input to the tomographic inversion. The

199   "seaward seismicity trend" (1,028 events) was relocated using a 1D velocity model of the

200   terrace (Dehler & Clowes, 1988) and OBS stations only, such that most wavepaths were

201   beneath the terrace and/or the adjacent Pacific plate (Fig. 2). Similarly, the "landward

202   seismicity trend" (1,680 events) was relocated using a 1D velocity model of the Haida

203   Gwaii islands (Spence & Asudeh, 1993) and land stations only. We used the double-difference

204   seismic tomography code `tomoDD10` (Zhang, 2003; Zhang & Thurber, 2003) to invert for

205   velocity structure only, keeping the earthquake hypocenters constant. In both `hypoDD`

206   and `tomoDD10` inversions, we employed both catalog differential times (`ph2dt`, Waldhauser

207   & Ellsworth, 2000) and cross-correlation differential times (Bostock et al., 2022).

208   The two weeks of data used in the previous step are dominated by seismicity as-

209   sociated with the aftermath of the 2012 M_w 7.8 event. To expand the 3D velocity model

210   into adjacent regions, we chose a subset of the full `Hypoinverse` earthquake catalog, en-

211   suring good spatial spread of seismicity. We selected earthquakes with root mean squared

212   traveltime residuals less than 1 s and location errors less than 5 km, taking only up to

213   100 earthquakes with the most phase picks across a 0.1° × 0.1° grid. We also included

214   all earthquakes constrained by OBS, swapping in their `hypoDD` relocations. The result-

215   ing catalog of the ~11,000 best-constrained earthquakes were then used to jointly invert

216   for 3D velocity structure and solve for earthquake hypocenters using `tomoDD10` and in-

217   corporating the output 3D velocity model from the previous step as the starting model.

218   The `tomoDD10` inversion was constrained with a total of 838,771 cross-correlation P- and

219   S-differential times, and 5,532,295 catalog P- and S-differential times. Finally, we relo-

220   cated the remaining ~42,000 earthquakes using the resulting 3D P- and S-wave veloc-

221 ity models. The final earthquake catalog has 51,562 earthquakes (see Supplementary Ma-
222 terials).

223   The primary focus of this study is the characterization and interpretation of seis-
224 micity in the region, and hence the velocity inversion was conducted primarily to improve
225 the earthquake locations. Given the small number of stations operating over most of the
226 period and the resulting limited resolution, we refrain from interpreting details in the
227 velocity structure beyond noting that they are generally consistent with previous mod-
228 els (Dehler & Clowes, 1988; Spence & Asudeh, 1993). We present Vp, Vs and Vp/Vs
229 cross sections in the Supplementary Materials.

3 Results

231   The full catalog clearly delineates two prominent near-parallel seismicity trends (Fig. 2),
232 both oriented about 8° counterclockwise from the previously mapped QCF surface trace
233 by Rohr (2015) and Brothers et al. (2020) (Fig. 3). The "landward seismicity trend" co-
234 incides with the QCF trace near 52.8°N but deviates along a trajectory that more closely
235 approaches the coast as one proceeds south. The "seaward seismicity trend" resides in
236 the Pacific plate, parallel to and immediately west of the bathymetric trough that bor-
237 ders the terrace. Because the dense seismicity (and greater average location uncertainty)
238 of the full catalog obscures spatial patterns, especially within the landward seismicity
239 trend, we will focus on the ~11,000 subset of best resolved earthquakes for which details
240 in the seismicity patterns are clearer (Fig. 2b). In the following subsections, we describe
241 the various earthquake clusters of interest, west to east, north to south. We also con-
242 sider the temporal dependence of seismicity over three separate intervals: before the 2012
243 M_w 7.8 event (Fig. 4a), during the aftershock period (Fig. 4b), and from 2016 onwards
244 when the seismicity appears to have leveled off (Fig. 4c,d).

3.1 Seaward Seismicity Trend

246   The seaward seismicity trend is strongly represented during the aftershock period,
247 with practically no detections prior to 2012 and much reduced levels from 2016 onwards
248 (Fig. 4). Despite the improved seismic network coverage following the 2012 M_w 7.8 earth-
249 quake, the lack of seismic activity prior to 2012 is likely robust. The persistence of mod-
250 estly elevated seismicity levels from 2016 onward may indicate that the activity here has

251   not yet returned to background levels. Earthquakes here are shallower than 10 km (Fig. 5),

252   suggesting that they reside primarily within Pacific oceanic crust. Kao et al. (2015) demon-

253   strate that the largest aftershocks have mostly normal mechanisms, consistent with an

254   origin related to bending of the oceanic plate. The trend can be divided into three clus-

255   ters (S1, S2, S3) (Fig. 2a), consistent with Farahbod and Kao (2015) who studied 1,229

256   aftershocks from the first week following the M_w 7.8 event. The southern cluster (S3)

257   is located around the northern terminus of the Revere-Dellwood fault (RDF) as defined

258   by Rohr (2015) (Fig. 4a). The northern limit of the seaward trend reaches ∼52.7°N, di-

259   rectly updip from the northernmost (∼52.85°N) end of the pronounced, deep (∼16 km)

260   seismicity of the landward trend (see Fig. 2).

3.2 Landward Seismicity Trend
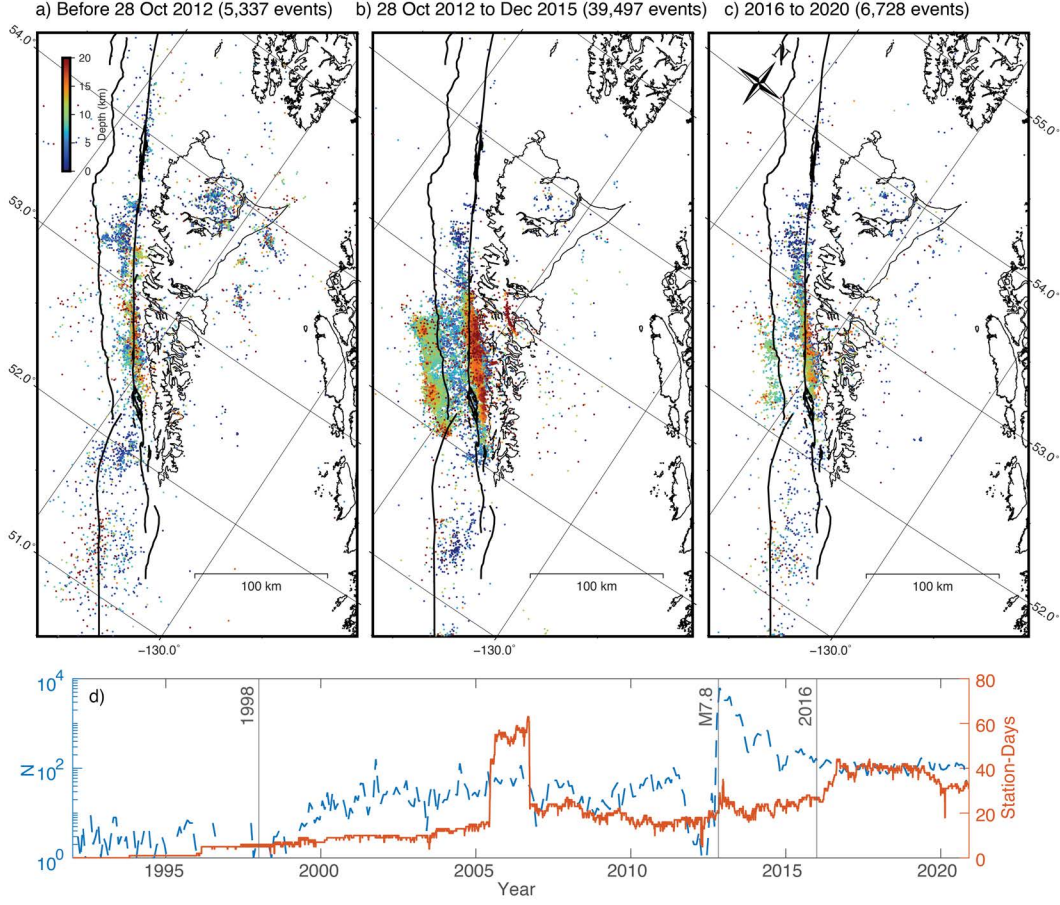
3.2.1 *Offshore Graham Island (Cluster L1)*

263   West of Graham Island, 53.0–53.5°N, seismicity along the QCF flips from predom-

264   inantly west of the mapped QCF surface trace (Brothers et al., 2020; Rohr et al., 2000),

265   to beneath the trace, and then back to the west, (cluster L1, Figs. 2,4). To the north of

266   53.5°N, less seismicity is detected (Fig. 6). Ristau et al. (2007) reported only strike-slip

267   moment tensors north of 53°N, whereas they mapped mostly thrust mechanisms to the

268   south. Moreover, the trend of the QCF trace bends clockwise north of 53.2°N, becom-

269   ing nearly parallel to the plate motion vector and consistent with diminished convergence

270   to the north (Rohr et al., 2000; Tréhu et al., 2015). Thus, ∼53.0–53.5°N appears to de-

271   fine the northern limit of the QCPB transpressive segment, consistent also with the north-

272   ern extent of the high bathymetric profile of the Queen Charlotte terrace.
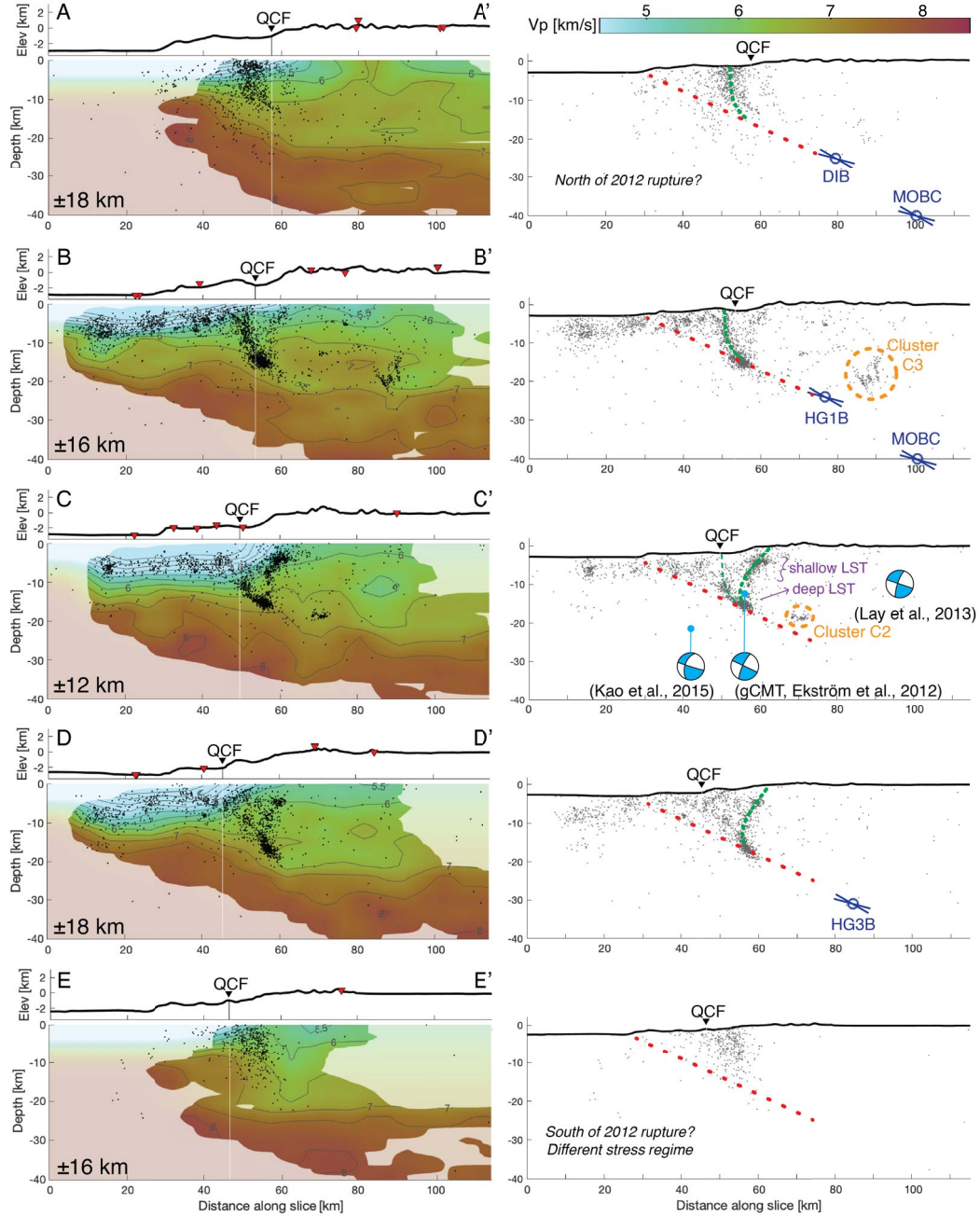
3.2.2 *Offshore Moresby Island (Clusters L2, L3, L4)*

274   The landward seismicity trend is densest and deepest west of Moresby Island, south

275   of 52.85°N (Fig. 2). Following the landward seismicity trend ∼80 km along-strike from

276   northwest to southeast, there is some lateral segmentation and a slight increase in max-

277   imum depth of seismicity from ∼16 to 20 km (H-H', Fig. 6). In map view, we identify

278   three clusters of note (clusters L2, L3, L4, Fig, 2).

279   Cluster L2 is a near-vertical structure, underlying the previously mapped QCF sur-

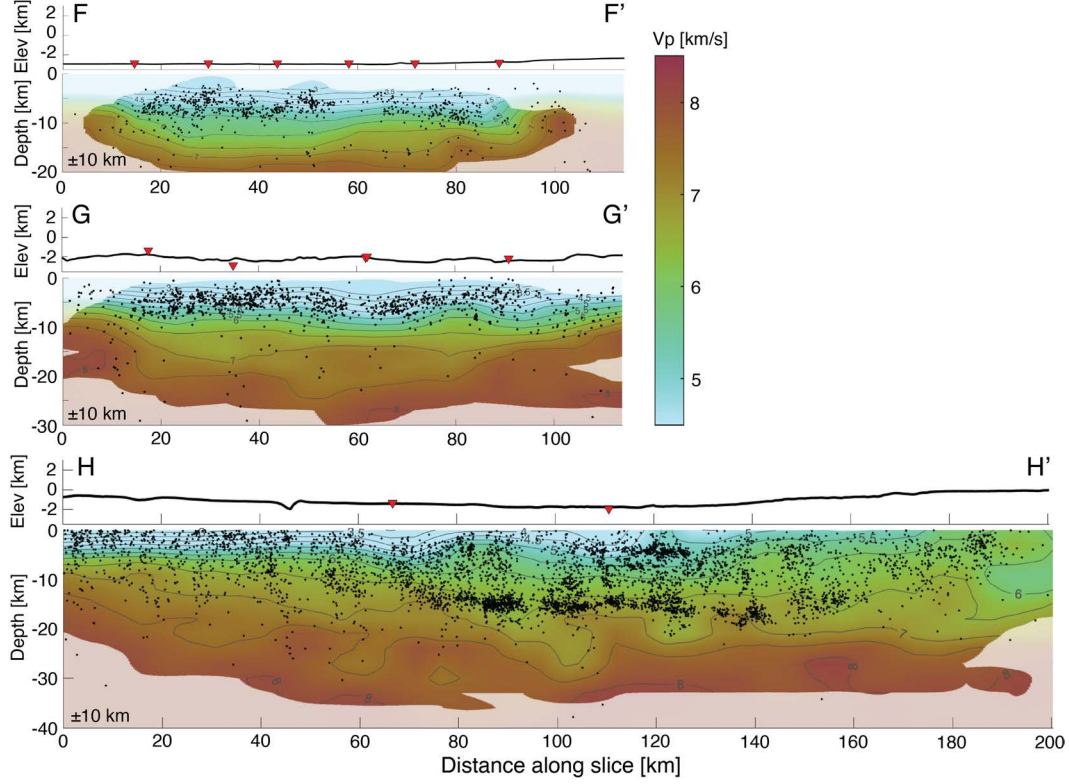280   face trace, with a maximum depth of ∼16 km, as evident on the across-QCF transect

Figure 4. Full seismic catalog split into three time periods: (a) prior to the 2012 M_w 7.8 earthquake, (b) from 28 October 2012 through December 2015, and (c) from 2016 through 2020, colored by depth with deepest plotted on top. The bottom plot (d) shows the station-days over time (solid orange line, right vertical axis) and number of earthquakes over time (dashed blue line, left vertical axis). 1998 signals the start of the automated catalog. M_w 7.8 labels the mainshock along the horizontal time axis and 2016 is when the seismicity seems to have leveled off. Increased station coverage in 2005–2006 is due to temporary stations of the Batholiths project (two lines of yellow triangles on the British Columbia mainland in Fig. 1) (Calkins et al., 2010). Mapped fault traces are from Brothers et al. (2020).

Figure 5. Across-fault cross-sections (see Fig. 3 for map view). Left column shows the Vp sections of the final velocity model (same color scale as Fig. 6). Seismicity projected onto the transects is from the ∼11,000 earthquake catalog and within the distances indicated on the bottom left corner of each panel. Inverted red triangles are stations. Black triangles are where the Queen Charlotte fault (QCF) trace as interpreted by Rohr (2015) intersects with the transects. Right column shows corresponding interpretations. Blue circles are receiver function depths to the top of a low velocity zone, with short blue lines representing 15° and 30° dips (Bustin et al., 2007; Gosselin et al., 2015). For reference purposes, we draw the red dotted lines from the trough to the receiver function depths. Green dotted lines are interpreted faults from the seismicity. Elevation has 2× vertical exaggeration on the left.

Figure 6. Along-fault cross-sections of the southern Queen Charlotte Plate Boundary: F-F', through the seaward seismicity trend; G-G', through the Queen Charlotte Terrace; and H-H', through the landward seismicity trend (see Fig. 3 for map view). Seismicity from the ∼11,000 earthquake subset, lying within 10 km of each transect, is plotted on the Vp sections of the final velocity model. Inverted red triangles are stations. Elevation has 2× vertical exaggeration.

281 (B-B', Fig. 5). Clusters L2 and L3 are separated by a paucity of seismicity that is most

282 apparent in the ∼11,000 subset catalog (Fig. 3). Along L3 and L4, the landward seis-

283 micity trend deviates eastwards from the previously mapped QCF surface trace, and ap-

284 proaching the Haida Gwaii coast to the south. Most evident on the cross-sectional view

285 of L3 (see 'shallow LST' and 'deep LST' in C-C', Fig. 5), we identify two subclusters that

286 overlie one another: a shallow subcluster dipping seaward from the surface to ∼10 km

287 depth, and a deep subcluster dipping landward at ∼8–17 km depths. Seismicity levels

288 decrease southward from L3 to L4. The southward continuation of the shallow and deep

289 subclusters of L3 persist into L4, with most events located east of the previously mapped

290 QCF surface trace (D-D', Fig. 5). Seismicity extends to ∼20 km depth in L4, such that

291 the landward seismicity trend slightly deepens from north to south (H-H', Fig. 6). Out-

292 side of the aftershock period (2012–2016), Clusters L2 and L3 exhibit some activity, but
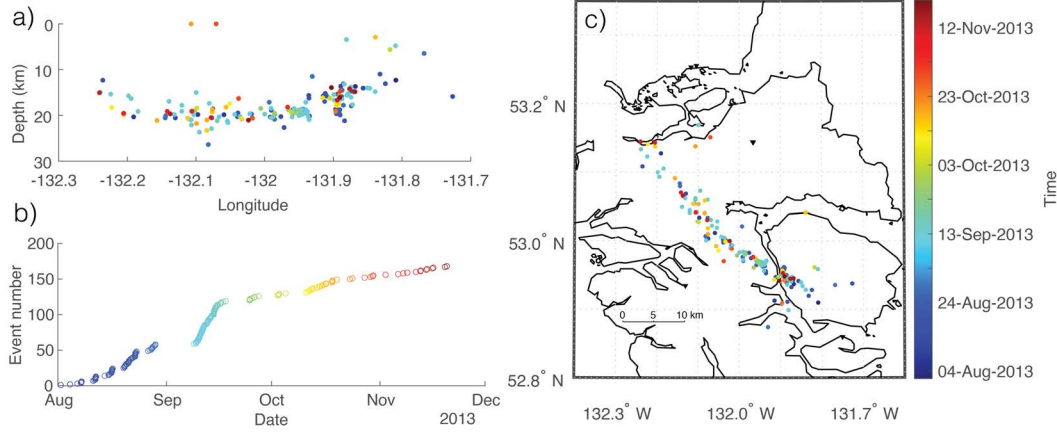
293 Cluster L4 registers almost no seismicity (Fig. 4).

294 ### 3.3 Other Earthquake Clusters

295 Beneath Graham Island and immediately east under the Hecate Strait, there are

296 concentrations of seismicity (clusters G1–G4) that have been previously identified and

297 hypothesized to be related to minor crustal faults by Bird (1999) and Ristau et al. (2007).

298 Near Moresby Island, we identify three clusters of interest, labelled C1, C2, C3 in Fig. 2.

299 Farther south, there is a shallow cluster of earthquakes near the Tuzo-Wilson seamounts

300 (T1 in Fig. 2) which Littel et al. (2023) discuss in detail.

301 Clusters C1 and C2 represent two small groups of earthquakes that are located just

302 off of the landward seismicity trend (Fig. 2). At ∼52.75°N, Cluster C1 extends west of

303 the QCF trace where most seismicity lies beneath the fault trace, and spreads subver-

304 tically from the surface to 12 km depth (Fig. 2). Cluster C2 falls just east of the land-

305 ward seismicity trend beneath Moresby Island near 52.65°N and concentrates at ∼20 km

306 depth (Fig. 2, C-C' in Figs. 3,5).

307 Farther landward at the northern end of Moresby Island, we observe a slightly ar-

308 cuate band of seismicity, subparallel to the two principal seismicity trends (Cluster C3,

309 Fig. 2; B-B' in Figs. 3,5). This feature comprises 168 earthquakes from August–December

310 2013, with magnitudes ≤∼3 and depths of 15–20 km, that were not reported in the CNSN

Figure 7. Linear seismicity trend beneath Moresby Island (C3, Fig. 2), colored in chronological order from blue to red, reveal no obvious spatiotemporal migration. a) Depth vs. Longitude profile. b) All earthquakes occurred between August and December 2013. c) Map view.

catalog (Fig. 7). Seismicity here exhibits no evidence for systematic spatiotemporal migration.

4 Discussion

4.1 Constraints on the Haida Gwaii thrust

The Haida Gwaii thrust (HGT) hosted the 2012 M_w 7.8 earthquake but there is debate on whether the underthrusting extends beneath the Haida Gwaii islands. Here we discuss the geometry of the LST and the seismicity clusters beneath Haida Gwaii and how they might provide insights into the extent of underthrusting.

In map view (Fig. 4b), aftershocks appear to delimit the coseismic rupture area (e.g., from Cassidy et al., 2014; Lay et al., 2013), but in cross-section (Fig. 5), there is little indication of the seismicity directly delineating a dipping HGT fault plane. Instead we infer a plausible geometry through consideration of additional constraints. We assume that the surface limit of the HGT coincides with the bathymetric trough, or the deformation front, just west of the terrace, and that the downdip extent is constrained by a low velocity zone identified by three independent receiver function studies, and interpreted as a proxy for the crust of the underthrust Pacific plate (Bustin et al., 2007; Gosselin et al., 2015; Smith et al., 2003). Receiver function modelling also suggests a slab dip of

15–30° (Fig. 5) (Gosselin et al., 2015), which is consistent with the range of dips (17–25°) from different moment tensor solutions of the 2012 M_w 7.8 earthquake (Ekström et al., 2012; Kao et al., 2015; Lay et al., 2013). For reference purposes, we draw red dotted lines dipping at 25° from the trough at the western edge of the QCT to 25 km depth, and note that landward extrapolation of this line exhibits a close correspondence with the top of the Pacific Plate inferred in the three receiver function studies. Moreover, the maximum depth of landward seismicity (i.e., the base of clusters L2, L3, L4) also aligns neatly with this reference line. The simplest explanation accommodating these and other constraints (the moment tensor fault plane geometry of the 2012 earthquake, its rupture area from standard earthquake scaling, the location of the bathymetric trough, and receiver function depths and dips) is that the HGT corresponds to the top of the Pacific Plate which underthrusts Haida Gwaii at an average dip near 25°. Furthermore, the deepest seismicity in L2, L3, L4 could be inferred to lie at the downdip terminus of the 2012 rupture and represent stress adjustments near the landward limit of the base of the QCT sliver in its role as a juncture in slip partitioning (e.g., Jarrard, 1986; Wang et al., 2015).

If the dipping low-velocity zone documented at a total of nine stations distributed across Graham and Moresby Islands (Smith et al., 2003; Bustin et al., 2007; Gosselin et al., 2015) has been erroneously attributed to the top of an underthrust Pacific Plate, as would be required by the interpretation of a no-slab model (e.g., Brothers et al., 2020), then the Pacific Plate may extend no farther landward than the deepest extensions of clusters L2, L3, L4. Both interpretations for the landward extent of Pacific plate are consistent with slip modeling of GNSS displacements (Nykolaishen et al., 2015), long period waveform and tsunami modeling (Lay et al., 2013), and downdip location (adjusted relative to centroid) of high frequency body wave radiation from teleseismic back projection (Lay et al., 2013), provided that any Pacific-North America relative plate motion below Haida Gwaii occurs independently and presumably aseismically (Wang et al., 2015).

Clusters C2 and C3 (C-C' and B-B' in Fig. 5) include deep (∼20 km) earthquakes beneath Moresby Island and may afford some constraint on the downdip extent of the HGT. Cluster C3 forms a slightly arcuate band that is subparallel to the two principal seismicity trends, suggesting it is somehow related to the stress regime of the tectonic margin. The continental Moho depths from receiver functions are modelled at ∼18 km just west of C3 and at ∼25 km to the east (HG1B, MOBC, Fig. 3), while the Moho depth

estimates nearest to C2 are at ∼18 km (HG1B, HG3B, Fig. 3) (Gosselin et al., 2015). Seismic refraction interpretations are generally consistent with these estimates and suggest that the Moho deepens eastward across Haida Gwaii from 21 to 28 km (Mackie et al., 1989; Spence & Asudeh, 1993). Accordingly, clusters C2 and C3 likely reside within the lowermost crust which must be sufficiently cool to support brittle deformation at depth. Here we consider several additional relevant observations. First, the nearest heat flow measurement is 47 mW/m^2 from a site some 10 km NW of C2 and 20 km SW of C3 (Hyndman et al., 1982). This value is comparable to those measured in south-central Vancouver Island (36–45 mW/m^2; Lewis et al., 1988) where the Juan de Fuca plate is of similar age to the Pacific plate off Haida Gwaii. Moreover, the Wrangellia terrane forms the North American crustal basement in both locations. Thermal modelling of heat flow observations in southern Vancouver Island (Gao & Wang, 2017) and Haida Gwaii (Wang et al., 2015) incorporating subduction yields similar temperatures near 350°C at 25 km depth. This depth corresponds to the maximum depth of earthquakes in Wrangellia on southern Vancouver Island (Savard et al., 2018). Thus we conclude that the locations and depths of clusters C2 and C3 are consistent with the presence of an underthrust Pacific Plate below Haida Gwaii.

4.2 Constraints on the Queen Charlotte fault system

Previous regional seismicity studies have inferred the QCF to approach the coast southward along Haida Gwaii but are based on more diffuse distributions of seismicity with larger location uncertainty (Bird, 1999; Ristau et al., 2007). Our seismicity relocation generally corroborates this, but also indicates increased complexity southward along Moresby Island. Seismicity appears adjacent to the mapped fault traces in the north (A-A' and B-B' in Fig. 3), then approaches the coast to the south, up to ∼10 km east of the previously mapped QCF surface trace. In particular, we identify a) significant departures from verticality, and b) multiple active strands, which we describe further below.

Acknowledging the poor constraints on the QCF geometry at depth, Wang et al. (2015) have hypothesized that it may dip steeply eastward off Moresby Island, noting that while the focal mechanism of the largest strike-slip earthquake in the region (1949 M_S 8.1) features a near-vertical fault plane, the 1970 M7.4 strike-slip event to the south has a northeast-dipping preferred nodal plane. Moreover, whereas a focal mechanism for

393 the 1929 M7.0 earthquake could not be calculated, a 1 m-high local tsunami was reported

394 which is consistent with some component of thrust (Cassidy et al., 2010; Rogers, 1983).

395 The steep apparent dip evident at the southern end of L1 (A-A', B-B', Fig. 5) is con-

396 sistent with the preferred fault plane (strike=327°, dip=82°) (Rogers, 1983) of the 1949

397 M_S 8.1 earthquake to the north which ruptured through this section (Bostwick, 1984;

398 Rogers, 1983).

399 We observe segmentation and along-strike complexity in the cross-sectional con-

400 centrations of seismicity along the landward seismicity trend. Along L2, we observe a

401 transition from primarily seaward vergence in the north to landward vergence in the south

402 (evident in cross-section view, B-B' and C-C', Fig. 5), accompanied by a paucity in earth-

403 quakes along-strike at ∼52.7°N (evident in map view, Figs. 3, 8b). Transects B-B', C-

404 C', and D-D' all display seismicity concentrations at depth. As discussed in section 4.1,

405 this feature is interpreted here as the merger of the QCF with the HGT, and is notably

406 absent along cross-sections A-A' and E-E' that lie outside the 2012 rupture zone. More-

407 over, some portion of this deep seismicity may represent aftershocks at the downdip limit

408 of the 2012 M_w 7.8 rupture.

409 Although the location of the previously mapped QCF trace off Graham Island and

410 farther north is clearly demarcated by its bathymetric expression (e.g., Brothers et al.,

411 2020; Rohr, 2015), its definition southward along Moresby Island becomes more com-

412 plex. The development of the QCT as a highly deformed sliver in response to compres-

413 sion means that there are multiple faults and folds evident on the seafloor that compli-

414 cate interpretation of the QCF in this region. Indeed, Rohr (2015) and Brothers et al.

415 (2020) mapped the QCF trace off Moresby Island based on seafloor geomorphology and

416 seismic reflection (see Fig. 3) with slightly different trajectories. The location of the QCF

417 trace is also characterized by a narrow, vertical low velocity zone down to about 6 km

418 depth (Dehler & Clowes, 1988; Riedel et al., 2021), but such structures are beyond the

419 resolution of our tomography.

420 The QCF traces as mapped by Rohr (2015) and Brothers et al. (2020) are iden-

421 tical north of 52.4°N and display deviations only southward of it (around D-D' in Figs. 3,

422 8d). In our own morphology assessment using available high-resolution multibeam swath

423 bathymetry (Barrie et al., 2013) and SeaMARC II sidescan sonar data (Davis et al., 1987),

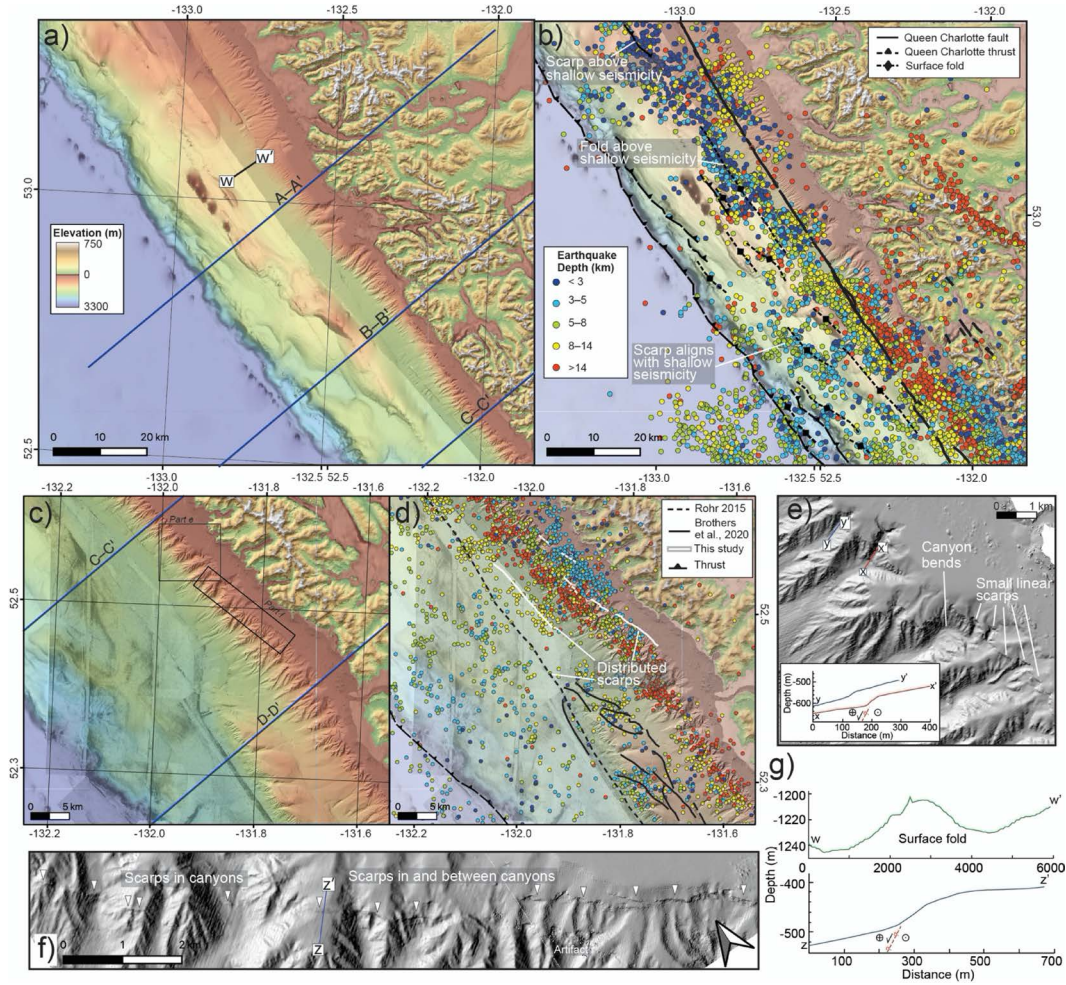424 the deviations begin south of ∼52.6°N (Fig. 8b,d). Figs. 8a,b provide an expanded view

425 of the bathymetry in the northern region and its relation to seismicity. Immediately south

426 of the left (compressional) step-over at 53.2°N, seismicity is dominantly shallow (<5 km)

427 and lies seaward of the QCF trace indicating that it is focused within the sediments of

428 the terrace. In particular, there appears to be an association between shallow earthquakes

429 and at least one fold crest that may be rooted by an out-of-sequence thrust fault (see

430 bathymetric profile in Fig. 8g across profile w-w' defined in Fig. 8a), though more data

431 are required to confirm this. As one proceeds southward into the rupture area of the 2012

432 event (midway between A-A' and B-B'), the average depth of seismicity increases and

433 deep (>14 km) events become more prevalent and organized immediately landward of

434 the principal QCF trace. Shallow seismicity persists seaward below the terrace with one

435 concentration in alignment with a scarp. This is also evident in cross-sectional view (Fig. 5)

436 where shallow seismicity is seemingly confined to a wedge-shaped block or sliver beneath

437 the terrace, possibly occurring on imbricate faults or flower structures, though further

438 data is needed to precisely identify the structures. Between B-B' and C-C', the paucity

439 in earthquakes along-strike at ∼52.7°N coincides with a discontinuity in our mapped faults,

440 which seems to mark the end of a well-defined single fault trace to the north. To the south-

441 east of C-C' (Figs. 8c,d), a principal QCF surface trace is more difficult to distinguish

442 and we interpret several distributed scarps. The most landward of these scarps skirts the

443 edge of the shelf for 15–20 km as evident in bathymetry both in and between canyons

444 (see Figs. 8e,f; profiles x-x', y-y', z-z'). This feature appears to be associated with and

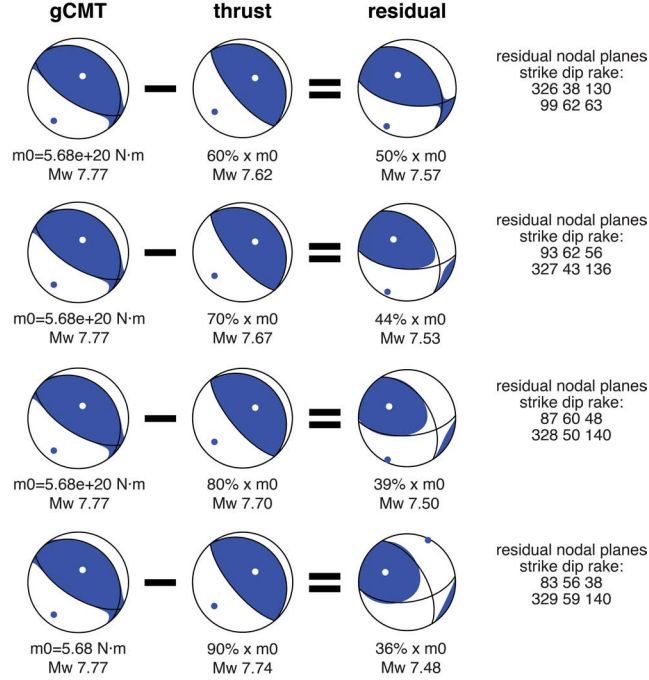445 could be a host structure to the corresponding section of the landward seismicity trend.

4.3 Reinterpreting postseismic earthquakes

447 Our new seismicity catalog hints that the QCF played a significant role in the 2012

448 M_w 7.8 event, since the landward seismicity trend adjacent to the QCF was especially

449 well represented during the aftershock period. In this section we explore the feasibility

450 of slip partitioning onto the QCF coeval with the 2012 earthquake using moment ten-

451 sor analysis. We present two possible, not necessarily mutually exclusive, endmember

452 interpretations for the aftershocks on the QCF, related to whether or not there was co-

453 seismic slip on the QCF.

454 In the first scenario, these aftershocks could be related to previously undocumented

455 coseismic slip shallower than ∼15 km on the QCF during the 2012 thrust mainshock.

456 At 15–20 km depth, they may define the downdip limit of the 2012 M_w 7.8 rupture, con-

Figure 8. Surface morphology and seismicity. a) Regional Global Multi-Resolution Topography bathymetry (Ryan et al., 2009) showing the morphology of the Queen Charlotte Terrace (QCT) offshore Graham Island, with cross-section lines of Fig. 5 in blue. The slightly darker area immediately offshore shows the limit of high-resolution bathymetry with a grid size of 5 m (Barrie et al., 2013). b) Same map as a) with interpretations from this study and earthquake epicenters colored by depth. Dashed black lines with teeth follow the trough representing the surface trace of the HGT, solid black lines are scarps associated with the Queen Charlotte Fault (QCF: dashed where inferred/uncertain), and dashed black lines with diamonds are the crests of surface folds. c) SeaMARC II sidescan sonar data (Davis et al., 1987) overlain by the high-resolution bathymetry showing the surface morphology offshore Moresby Island. d) Same map as c) with earthquakes colored by depth, mapped strands of the QCF from previous studies, and new strands identified in this study. e) and f) are shaded relief maps from the high-resolution bathymetry, showing scarps in the canyons and inset shows bathymetric profiles across scarps. g) Bathymetric profiles across a subtle surface fold that aligns with shallow seismicity north of section A-A' (top) and across a section of the scarp in part f) (bottom). Topography on Haida Gwaii islands is the 30-m Advanced Spaceborne Thermal Emission and Reflection Radiometer (ASTER) global dataset.

Figure 9. Illustration of theoretical partitioning of the gCMT moment tensor solution into pure thrust and residual events, assuming that the seismic moment of the thrust event is 60–90 % of the composite moment tensor.

sistent with the distribution of coseismic HGT slip (3–6 m slip contours from Lay et al., 2013), and may also coincide with the source of the coseismic high frequency body wave energy modeled by Lay et al. (2013).

In the second scenario, the landward seismicity trend does not include aftershocks to coseismic slip on the QCF per se, but instead manifests significant aseismic afterslip on the QCF. Nykolaishen et al. (2015) hinted at the possibility of induced aseismic slip on the deeper QCF based on the observed southeasterly postseismic displacements at GNSS stations on the southern half of Moresby Island. Postseismic strike-slip motion, especially at 10–20 km depth, is also supported by Coulomb stress estimates of Hobbs et al. (2015) and the activity of repeating earthquakes documented by Hayward and Bostock (2017).

To explore the first scenario, we perform simple tests of whether the seismic moment tensor of the 2012 M_w 7.8 earthquake can be partitioned into a pure thrust event on the HGT and a concurrent strike-slip event on the QCF (Fig. 9). We investigate the

non-double-couple gCMT solution of the 2012 mainshock, noting that the non-double-couple nature of a seismic source can arise from fault complexity such as events of differing geometry occurring close together in space and time (e.g., Julian et al., 1998). We assume a pure thrust main earthquake with a strike paralleling both the seaward and landward seismicity trends (strike=320°, dip=18°, rake=90°). Subtracting this theoretical thrust moment tensor at a range of magnitudes, (corresponding to between 60–90% of the total seismic moment of $5.68 \times 10^{(20)}$N-m) from the gCMT solution, we obtain a suite of residual moment tensors. Each of these is observed to have an oblique mechanism with a right-lateral nodal plane close to the strike of the QCF, dipping moderately northeastward at 40–60°. The higher the seismic moment of the thrust event contribution, the steeper the fault plane dip of the residual moment tensor, with a maximum dip of ∼60° at ∼90% of M_0, consistent at least qualitatively with our inference of a variably dipping QCF.

The modeling exercise suggests that, in principle, the slip of the M_w 7.8 earthquake could have been partitioned into near-simultaneous thrust and strike-slip events along the HGT and QCF, respectively. In particular, we note that the location of the QCF surface trace is bathymetrically well defined north of ∼52.6°N (where Rohr (2015), Brothers et al. (2020), and our bathymetric interpretations are in fair agreement, southwards to between B-B' and C-C'), and that it sits systematically seaward of the deeper (16–20 km) seismicity concentrations profiled in Fig. 5. On the assumption that the principal QCF connects the surface trace with the deep landward seismicity trend, it would dip ∼60° NE on C-C', which is just within the range of dips from the modeling exercise (farther north, the structure would be steeper than suggested by the modeling). One potential caveat is that if coseismic slip did occur along this structure, it would display little evidence for aftershock activity at shallower levels, as is the case on the main thrust plane. However, a scarcity of shallow aftershock seismicity is a common characteristic of large, continental strike-slip sequences, as exemplified by the well-characterized 2000 M_w 6.8 Tottori, Japan, 2003 M_w 6.6 Bam, Iran, 2008 M_w 7.9 Wenchuan, China, 2014 M_w 6.1 South Napa, USA, and 2020 M_w 6.8 Elazığ, Turkey earthquakes (Semmane et al., 2005; Jackson et al., 2006; Tong et al., 2010; Wei et al., 2015; Pousse-Beltran et al., 2020)

GNSS-based modeling of postseismic deformation reveals afterslip on the HGT, downdip of the mainshock, and small right-lateral afterslip on the QCF (Guns et al., 2021; Tian et al., 2021). Repeating earthquakes also indicate thrust and strike-slip afterslip (Hayward

504 & Bostock, 2017), and so both suites of observations are consistent with the second sce-

505 nario. However, neither approach supplies strong constraints during the coseismic pe-

506 riod since there was only one nearby continuous GNSS station running during the earth-

507 quake, and small, repeating earthquakes would be obscured by the mainshock and ear-

508 lier larger aftershocks. Extrapolating the accelerated rates of afterslip from repeating earth-

509 quakes in the days and weeks immediately following the mainshock (Hayward & Bostock,

510 2017) backwards in time supports the possibility of high coseismic slip rates on the QCF

511 during the thrust mainshock, as in the first scenario.

4.4 Tectonic and hazard implications

513 While the QCPB comprises a simple and well-defined fault zone in the north along

514 coastal Alaska (e.g., Brothers et al., 2020), our observations together with those of Tréhu

515 et al. (2015) demonstrate that its expression becomes increasingly complex offshore Haida

516 Gwaii. The 1949 M_S 8.1 earthquake ruptured mostly northwestwards (from surface wave

517 directivity and most of the aftershocks occurred to the north) with a smaller component

518 southeastwards (based on five aftershocks southward along the margin, down to 52.0°N)

519 (Bostwick, 1984). This uneven rupture propagation might be due to the increased com-

520 plexity and fault segmentation to the south, though a preferred directivity arising from

521 a bimaterial contrast across the QCF has also been suggested (Aderhold & Abercrom-

522 bie, 2015). In light of our results, we may reinterpret the southernmost 1949 aftershocks

523 to be stress adjustments on adjacent faults that did not slip during the mainshock. In-

524 stead we speculate that the 1949 M_S 8.1 strike-slip event ruptured through the QCF sec-

525 tion dipping steeply landward but no farther southward than ∼52.7°N (between B-B'

526 and C-C' in Fig. 5) where the fault geometry becomes more complex. However, it is im-

527 portant to note, as demonstrated by multi-fault strike-slip earthquakes such as the 2010

528 M_w 7.2 El Mayor-Cucapah and the 2016 M_w 7.8 Kaikōura earthquakes, that fault seg-

529 mentation would not necessarily arrest all fault ruptures (e.g., Fletcher et al., 2014; Ham-

530 ling, 2020).

531 The lack of HGT seismicity before the 2012 mainshock might imply that the HGT

532 was locked, at least partially, given that repeating earthquake activity suggested some

533 degree of aseismic slip (Hayward & Bostock, 2017). Furthermore, the lack of aftershocks

534 demarcating the HGT fault plane suggest a near-total stress drop which has been pro-

535 posed for megathrust events (e.g., Wetzler et al., 2018). On the other hand, fault lock-

ing on the QCF is less straightforward. We have shown that the QCF could have been either locked or slipping during the 2012 mainshock. If the QCF slipped as part of the mainshock, then the sliver would have moved northward in addition to updip as the hanging wall of the HGT, but without GNSS recordings on the terrace this cannot be confirmed. The 2012 M_w 7.8 thrust component likely unclamped the QCF as the sliver moved updip, thus facilitating postseismic motion on the QCF evident in the increase in the number of earthquakes in the landward seismicity trend during the aftershock period.

The Puysegur subduction zone is frequently cited as an example of subduction initiation (Collot et al., 1995; Stern & Gerya, 2018; Gurnis et al., 2019; Lallemand & Arcay, 2021; Shuck et al., 2021) and is an analogue to the QCPB at Haida Gwaii (Hyndman, 2015). Both regions involve young oceanic lithosphere juxtaposed against a continental plate in a transpressive setting. At the Puysegur subduction zone, oblique motion is partitioned along a forearc sliver between the Puysegur Trench and the nearby right-lateral Puysegur Fault (Hayes et al., 2009), analogous to the QCT, HGT, and QCF. The convergence rate at Puysegur is ∼18 mm/yr (Lebrun et al., 2003), similar to the upper bound of convergence estimates at QCPB (6–18 mm/yr). Note that in the subduction context, obliquity is commonly defined as the angle between the plate convergence vector and the normal to the trench, such that zero obliquity means pure convergence. Both Puysegur and QCPB are examples of highly oblique settings, with obliquity of 60° and 70–84°, respectively— the latter of distinctly higher obliquity. Shuck et al. (2021) argued that compressive strike-slip settings may play an important role in subduction initiation and thus a key component in realizing the Wilson cycle. The QCPB at Haida Gwaii provides support for this contention and our observations provide insights into details of slip partitioning in the transformation from strike-slip deformation to sustained subduction.

5 Conclusions

We have employed automatic detection and joint hypocenter-velocity inversion to yield both the largest and highest precision earthquake location catalog for Haida Gwaii assembled to date for the period 1998-2020 that includes the M_w 7.8 October 2012 event. Our relocated earthquakes reveal a number of interesting features:

1. Seismicity is dominated by two parallel strands: a seaward strand just west of the deformation front within the Pacific plate, and a landward strand that runs close

to the coast of Moresby island; both of which outline the rupture area of the 2012 M_w 7.8 earthquake. The former has been previously characterized as the response to bending stresses in the Pacific plate. The latter defines a complex system involving multiple structures, the most prominent of which lies offset from the previously mapped QCF surface trace and appears to extend down to seismicity concentrations between 15 and 20 km depth, which plausibly represent stress concentrations at the juncture of slip partitioning between the Pacific and North American plates and the QCT sliver.

2. It is notable that little seismicity locates directly beneath the previously mapped bathymetric QCF trace, a relation that persists north of the 2012 rupture zone to offshore Graham Island. Seismicity in this region appears to be related to shallower fault structures within the QCT associated with uplift and shortening of the sliver in response to highly oblique Pacific North America plate motion.

3. At ∼52.7°N, there is a paucity in earthquakes along-strike, a discontinuity in our mapped fault segments, a change from seaward vergence to landward vergence of the seismicity structure from north to south, and a shift from a single well-identified fault trace to the north to multiple fault segments to the south. These features highlight fault complexity south of ∼52.7°N.

4. We note two previously undocumented isolated deep (up to ∼20 km) clusters of seismicity below Haida Gwaii east of the 2012 rupture zone, one of which is approximately linear and extends over ∼40 km and parallels the two main seismicity trends. Their presence is consistent with a significant landward extension of the underthrust Pacific plate below Haida Gwaii, lending strong support to the notion that the QCBP is an incipient subduction zone.

5. The marked increase and subsequent decrease in microseismicity along the landward trend over the two years immediately following the 2012 event may signify aftershocks to coseismic rupture (M_w 7.5–7.6) along a NE-dipping QCF or, alternatively may represent larger scale postseismic aseismic slip.

6. Modelling the 2012 moment tensor (gCMT) as a combination of pure dip slip along a thrust plane defined by the strike of the seaward and landward seismicity trends and a residual component, allows the possibility of significant (M_w 7.5) coseismic strike-slip motion along a QCF that dips to the NE at ∼40–60°. This scenario is plausible if the QCF surface trace, as defined bathymetrically, joins the landward

seismicity concentration at depth (16–20 km). Like the main thrust event, it would imply little or no aftershock activity at shallow levels.

Open Research Section

All seismic data were obtained from the Natural Resources Canada (publicly accessible via `ftp://ftp.seismo.nrcan.gc.ca`), and the EarthScope Consortium Web Services (`https://service.iris.edu/`), including the following seismic networks: AK (Alaska Earthquake Center, Univ. of Alaska Fairbanks, 1987); C8, CN, PO (Natural Resources Canada, 1975); TA (IRIS Transportable Array, 2003); XY (Ken Dueker & George Zandt, 2005).

References

Aderhold, K., & Abercrombie, R. (2015). Seismic rupture on an oceanic–continental plate boundary: Strike-slip earthquakes along the Queen Charlotte–Fairweather Fault. *Bulletin of the Seismological Society of America*, *105*(2B), 1129–1142. doi: https://doi.org/10.1785/0120140227

Alaska Earthquake Center, Univ. of Alaska Fairbanks. (1987). *Alaska geophysical network.* International Federation of Digital Seismograph Networks. Retrieved from `https://www.fdsn.org/networks/detail/AK/` doi: 10.7914/SN/AK

Barrie, J. V., Conway, K. W., & Harris, P. T. (2013). The Queen Charlotte fault, British Columbia: Seafloor anatomy of a transform fault and its influence on sediment processes. *Geo-Marine Letters*, *33*, 311–318. doi: https://doi.org/10.1007/s00367-013-0333-3

Bird, A. L. (1999). *Earthquakes in the Queen Charlotte Islands region: 1982-1996.* (Unpublished doctoral dissertation). University of Victoria.

Bostock, M., Plourde, A., Drolet, D., & Littel, G. (2022). Multichannel alignment of S waves. *Bulletin of the Seismological Society of America*, *112*(1), 133–142. doi: https://doi.org/10.1785/0120210076

Bostwick, T. K. (1984). *A re-examination of the August 22, 1949 Queen Charlotte earthquake* (Doctoral dissertation, University of British Columbia). doi: https://doi.org/10.14288/1.0052501

Brothers, D. S., Miller, N. C., Barrie, J. V., Haeussler, P. J., Greene, H. G., Andrews, B. D., . . . Dartnell, P. (2020). Plate boundary localization, slip-rates and rupture segmentation of the Queen Charlotte Fault based on submarine tectonic geomorphology. *Earth and Planetary Science Letters*, *530*, 115882. doi: https://doi.org/10.1016/j.epsl.2019.115882

Bustin, A., Hyndman, R., Kao, H., & Cassidy, J. (2007). Evidence for underthrusting beneath the Queen Charlotte Margin, British Columbia, from teleseismic receiver function analysis. *Geophysical Journal International*, *171*(3), 1198–1211. doi: https://doi.org/10.1111/j.1365-246X.2007.03583.x

Calkins, J. A., Zandt, G., Girardi, J., Dueker, K., Gehrels, G. E., & Ducea, M. N. (2010). Characterization of the crust of the Coast Mountains Batholith, British Columbia, from P to S converted seismic waves and petrologic modeling. *Earth and Planetary Science Letters*, *289*(1-2), 145–155. doi: https://doi.org/10.1016/j.epsl.2009.10.037

Cassidy, J. F., Rogers, G. C., & Hyndman, R. D. (2014). An overview of the 28 October 2012 M w 7.7 earthquake in Haida Gwaii, Canada: a tsunamigenic thrust event along a predominantly strike-slip margin. *Pure and Applied Geophysics*, *171*, 3457–3465. doi: https://doi.org/10.1007/s00024-014-0775-1

Cassidy, J. F., Rogers, G. C., Lamontagne, M., Halchuk, S., & Adams, J. (2010). Canada's Earthquakes: 'The Good, the Bad, and the Ugly'. *Geoscience Canada*, *37*(1), 1–16.

Collot, J.-Y., Lamarche, G., Wood, R. A., Delteil, J., Sosson, M., Lebrun, J.-F., & Coffin, M. F. (1995). Morphostructure of an incipient subduction zone along a transform plate boundary: Puysegur Ridge and Trench. *Geology*, *23*(6), 519–522. doi: https://doi.org/10.1130/0091-7613(1995)023⟨0519:

MOAISZ⟩2.3.CO;2

Comte, D., Farias, M., Roecker, S., & Russo, R.   (2019).   The nature of the
        subduction wedge in an erosive margin: Insights from the analysis of af-
        tershocks of the 2015 Mw 8.3 Illapel earthquake beneath the Chilean
        Coastal Range.   *Earth and Planetary Science Letters*, *520*, 50–62.   doi:
        https://doi.org/10.1016/j.epsl.2019.05.033

Davis, E. E., Currie, R. G., & Sawyer, B. (1987). *Acoustic imagery, southern Queen
        Charlotte margin.* Geological Survey of Canada. (Preliminary Map 10-1987, 1
        sheet) doi: https://doi.org/10.4095/133936

Dehler, S. A., & Clowes, R. M.   (1988).   The Queen Charlotte Islands refraction
        project. Part I. The Queen Charlotte Fault Zone.   *Canadian Journal of Earth
        Sciences*, *25*(11), 1857–1870. doi: https://doi.org/10.1139/e88-175

DeMets, C., Gordon, R. G., & Argus, D. F.   (2010).   Geologically current plate mo-
        tions. *Geophysical journal international*, *181*(1), 1–80. doi: https://doi.org/10
        .1111/j.1365-246X.2009.04491.x

DeMets, C., & Merkouriev, S.   (2016).   High-resolution reconstructions of Pacific–
        North America plate motion: 20 Ma to present.   *Geophysical Journal Interna-
        tional*, *207*(2), 741–773. doi: https://doi.org/10.1093/gji/ggw305

Ekström, G., Nettles, M., & Dziewoński, A. (2012). The global CMT project 2004–
        2010: Centroid-moment tensors for 13,017 earthquakes.   *Physics of the Earth
        and Planetary Interiors*, *200*, 1–9. doi: https://doi.org/10.1016/j.pepi.2012.04
        .002

Farahbod, A. M., & Kao, H.   (2015).   Spatiotemporal distribution of events dur-
        ing the first week of the 2012 Haida Gwaii aftershock sequence. *Bulletin of the
        Seismological Society of America*, *105*(2B), 1231–1240. doi: https://doi.org/10
        .1785/0120140173

Fletcher, J. M., Teran, O. J., Rockwell, T. K., Oskin, M. E., Hudnut, K. W.,
        Mueller, K. J., . . . González-García, J.   (2014).   Assembly of a large earth-
        quake from a complex fault system: Surface rupture kinematics of the 4 April
        2010 El Mayor–Cucapah (Mexico) Mw 7.2 earthquake.   *Geosphere*, *10*(4),
        797–827. doi: https://doi.org/10.1130/GES00933.1

Gao, X., & Wang, K. (2017). Rheological separation of the megathrust seismogenic
        zone and episodic tremor and slip. *Nature*, *543*(7645), 416–419. doi: https://

doi.org/10.1038/nature21389

Gosselin, J. M., Cassidy, J. F., & Dosso, S. E. (2015). Shear-wave velocity structure in the vicinity of the 2012 M w 7.8 Haida Gwaii earthquake from receiver function inversion. *Bulletin of the Seismological Society of America*, *105*(2B), 1106–1113. doi: https://doi.org/10.1785/0120140171

Guns, K., Pollitz, F., Lay, T., & Yue, H. (2021). Exploring GPS observations of postseismic deformation following the 2012 MW7. 8 Haida Gwaii and 2013 MW7. 5 Craig, Alaska earthquakes: Implications for viscoelastic Earth structure. *Journal of Geophysical Research: Solid Earth*, *126*(7), e2021JB021891. doi: https://doi.org/10.1029/2021JB021891

Gurnis, M., Van Avendonk, H., Gulick, S. P., Stock, J., Sutherland, R., Hightower, E., . . . others (2019). Incipient subduction at the contact with stretched continental crust: The Puysegur Trench. *Earth and Planetary Science Letters*, *520*, 212–219. doi: https://doi.org/10.1016/j.epsl.2019.05.044

Hamling, I. J. (2020). A review of the 2016 Kaikōura earthquake: insights from the first 3 years. *Journal of the Royal Society of New Zealand*, *50*(2), 226–244. doi: https://doi.org/10.1080/03036758.2019.1701048

Hayes, G. P., Furlong, K. P., & Ammon, C. J. (2009). Intraplate deformation adjacent to the macquarie ridge south of new zealand—the tectonic evolution of a complex plate boundary. *Tectonophysics*, *463*(1-4), 1–14. doi: https://doi.org/10.1016/j.tecto.2008.09.024

Hayward, T. W., & Bostock, M. G. (2017). Slip behavior of the queen Charlotte plate boundary before and after the 2012, MW 7.8 Haida Gwaii earthquake: evidence from repeating earthquakes. *Journal of Geophysical Research: Solid Earth*, *122*(11), 8990–9011. doi: https://doi.org/10.1002/2017JB014248

Hobbs, T., Cassidy, J., Dosso, S., & Brillon, C. (2015). Coulomb Stress Changes Following the 2012 M w 7.8 Haida Gwaii, Canada, Earthquake: Implications for Seismic Hazard. *Bulletin of the Seismological Society of America*, *105*(2B), 1253–1264. doi: https://doi.org/10.1785/0120140158

Hyndman, R. (2015). Tectonics and structure of the Queen Charlotte fault zone, Haida Gwaii, and large thrust earthquakes. *Bulletin of the Seismological Society of America*, *105*(2B), 1058–1075. doi: https://doi.org/10.1785/0120140181

Hyndman, R., Lewis, T., Wright, J., Burgess, M., Chapman, D., & Yamano, M. (1982). Queen Charlotte fault zone: Heat flow measurements. *Canadian Journal of Earth Sciences*, *19*(8), 1657–1669. doi: https://doi.org/10.1139/e82-141

IRIS Transportable Array. (2003). *Usarray transportable array.* International Federation of Digital Seismograph Networks. Retrieved from `https://www.fdsn.org/networks/detail/TA/` doi: 10.7914/SN/TA

Jackson, J., Bouchon, M., Fielding, E., Funning, G., Ghorashi, M., Hatzfeld, D., ... Wright, T. (2006). Seismotectonic, rupture process, and earthquake-hazard aspects of the 2003 December 26 Bam, Iran, earthquake. *Geophysical Journal International*, *166*(3), 1270–1292. doi: https://doi.org/10.1111/j.1365-246X.2006.03056.x

Jarrard, R. D. (1986). Relations among subduction parameters. *Reviews of Geophysics*, *24*(2), 217–284. doi: https://doi.org/10.1029/RG024i002p00217

Julian, B. R., Miller, A. D., & Foulger, G. (1998). Non-double-couple earthquakes 1. Theory. *Reviews of Geophysics*, *36*(4), 525–549. doi: https://doi.org/10.1029/98RG00716

Kao, H., Shan, S.-J., & Farahbod, A. M. (2015). Source characteristics of the 2012 Haida Gwaii earthquake sequence. *Bulletin of the Seismological Society of America*, *105*(2B), 1206–1218. doi: https://doi.org/10.1785/0120140165

Ken Dueker, & George Zandt. (2005). *Magma accretion and the formation of batholiths.* International Federation of Digital Seismograph Networks. Retrieved from `https://www.fdsn.org/networks/detail/XY_2005/` doi: 10.7914/SN/XY_2005

Kushnir, A., Lapshin, V., Pinsky, V., & Fyen, J. (1990). Statistically optimal event detection using small array data. *Bulletin of the seismological society of america*, *80*(6B), 1934–1950. doi: https://doi.org/10.1785/BSSA08006B1934

Lallemand, S., & Arcay, D. (2021). Subduction initiation from the earliest stages to self-sustained subduction: Insights from the analysis of 70 Cenozoic sites. *Earth-Science Reviews*, *221*, 103779. doi: https://doi.org/10.1016/j.earscirev.2021.103779

Lanza, F., Chamberlain, C., Jacobs, K., Warren-Smith, E., Godfrey, H., Kortink, M., ... Eberhart-Phillips, D. (2019). Crustal fault connectivity of the Mw

7.8 2016 Kaikōura earthquake constrained by aftershock relocations. *Geophysical Research Letters*, *46*(12), 6487–6496. doi: https://doi.org/10.1029/2019GL082780

Lay, T., Ye, L., Kanamori, H., Yamazaki, Y., Cheung, K. F., Kwong, K., & Koper, K. D. (2013). The October 28, 2012 Mw 7.8 Haida Gwaii underthrusting earthquake and tsunami: Slip partitioning along the Queen Charlotte Fault transpressional plate boundary. *Earth and Planetary Science Letters*, *375*, 57–70. doi: https://doi.org/10.1016/j.epsl.2013.05.005

Lebrun, J.-F., Lamarche, G., & Collot, J.-Y. (2003). Subduction initiation at a strike-slip plate boundary: The Cenozoic Pacific-Australian plate boundary, south of New Zealand. *Journal of Geophysical Research: Solid Earth*, *108*(B9). doi: https://doi.org/10.1029/2002JB002041

Lewis, T., Bentkowski, W., Davis, E., Hyndman, R., Souther, J., & Wright, J. (1988). Subduction of the Juan de Fuca plate: thermal consequences. *Journal of Geophysical Research: Solid Earth*, *93*(B12), 15207–15225. doi: https://doi.org/10.1029/JB093iB12p15207

Littel, G., Bostock, M., Schaeffer, A., & Roecker, S. (2023). Microplate evolution in the Queen Charlotte triple junction & Explorer region: New insights from microseismicity. *Tectonics*, *42*, e2022TC007494. doi: https://doi.org/10.1029/2022TC007494

Mackie, D., Clowes, R., Dehler, S., Ellis, R., & Morel-À-l'Huissier, P. (1989). The Queen Charlotte Islands refraction project. Part II. Structural model for transition from Pacific plate to North American plate. *Canadian Journal of Earth Sciences*, *26*(9), 1713–1725. doi: https://doi.org/10.1139/e89-146

Natural Resources Canada. (1975). *Canadian national seismograph network.* International Federation of Digital Seismograph Networks. Retrieved from `https://www.fdsn.org/networks/detail/CN/` doi: 10.7914/SN/CN

Nykolaishen, L., Dragert, H., Wang, K., James, T. S., & Schmidt, M. (2015). GPS observations of crustal deformation associated with the 2012 M w 7.8 Haida Gwaii earthquake. *Bulletin of the Seismological Society of America*, *105*(2B), 1241–1252. doi: https://doi.org/10.1785/0120140177

Pisarenko, V., Kushnir, A., & Savin, I. (1987). Statistical adaptive algorithms for estimation of onset moments of seismic phases. *Physics of the Earth and Plane-*

795   *tary Interiors*, *47*, 4–10. doi: https://doi.org/10.1016/0031-9201(87)90062-8

796   Pousse-Beltran, L., Nissen, E., Bergman, E. A., Cambaz, M. D., Gaudreau, É.,

797   Karasözen, E., & Tan, F.   (2020).   The 2020 M w 6.8 Elazığ (Turkey) earth-

798   quake reveals rupture behavior of the East Anatolian Fault.   *Geophysical*

799   *Research Letters*, *47*(13), e2020GL088136.   doi: https://doi.org/10.1029/

800   2020GL088136

801   Rawles, C., & Thurber, C.   (2015).   A non-parametric method for automatic de-

802   termination of P-wave and S-wave arrival times: application to local micro

803   earthquakes.   *Geophysical Journal International*, *202*(2), 1164–1179.   doi:

804   https://doi.org/10.1093/gji/ggv218

805   Riddihough, R., Currie, R., & Hyndman, R. (1980). The Dellwood Knolls and their

806   role in triple junction tectonics off northern Vancouver Island. *Canadian Jour-*

807   *nal of Earth Sciences*, *17*(5), 577–593. doi: https://doi.org/10.1139/e80-057

808   Riedel, M., Yelisetti, S., Papenberg, C., Rohr, K., Côté, M., Spence, G., . . . James,

809   T. (2021). Seismic velocity structure of the Queen Charlotte terrace off west-

810   ern Canada in the region of the 2012 Haida Gwaii Mw 7.8 thrust earthquake.

811   *Geosphere*, *17*(1), 23–38. doi: https://doi.org/10.1130/GES02258.1

812   Ristau, J., Rogers, G. C., & Cassidy, J. F.   (2007).   Stress in western Canada from

813   regional moment tensor analysis.   *Canadian Journal of Earth Sciences*, *44*(2),

814   127–148. doi: https://doi.org/10.1139/e06-057

815   Roecker, S., Thurber, C., Roberts, K., & Powell, L.   (2006).   Refining the image

816   of the San Andreas Fault near Parkfield, California using a finite difference

817   travel time computation technique.   *Tectonophysics*, *426*(1-2), 189–205.   doi:

818   https://doi.org/10.1016/j.tecto.2006.02.026

819   Rogers, G. C.   (1983).   *Seismotectonics of British Columbia* (Doctoral dissertation,

820   University of British Columbia). doi: https://doi.org/10.14288/1.0052938

821   Rohr, K. M. (2015). Plate boundary adjustments of the southernmost Queen Char-

822   lotte fault.   *Bulletin of the Seismological Society of America*, *105*(2B), 1076–

823   1089. doi: https://doi.org/10.1785/0120140162

824   Rohr, K. M., Scheidhauer, M., & Trehu, A. M.   (2000).   Transpression between two

825   warm mafic plates: The Queen Charlotte Fault revisited.   *Journal of Geophys-*

826   *ical Research: Solid Earth*, *105*(B4), 8147–8172. doi: https://doi.org/10.1029/

827   1999JB900403

828 Ryan, W. B., Carbotte, S. M., Coplan, J. O., O'Hara, S., Melkonian, A., Arko, R.,

829 . . . Zemsky, R. (2009). Global multi-resolution topography synthesis. *Geo-*

830 *chemistry, Geophysics, Geosystems*, *10*(3). doi: https://doi.org/10.1029/

831 2008GC002332

832 Savard, G., Bostock, M. G., & Christensen, N. I. (2018). Seismicity, metamorphism,

833 and fluid evolution across the northern Cascadia fore arc. *Geochemistry,*

834 *Geophysics, Geosystems*, *19*(6), 1881–1897. doi: https://doi.org/10.1029/

835 2017GC007417

836 Semmane, F., Cotton, F., & Campillo, M. (2005). The 2000 Tottori earthquake:

837 A shallow earthquake with no surface rupture and slip properties controlled

838 by depth. *Journal of Geophysical Research: Solid Earth*, *110*(B3). doi:

839 https://doi.org/10.1029/2004JB003194

840 Shuck, B., Van Avendonk, H., Gulick, S. P., Gurnis, M., Sutherland, R., Stock, J.,

841 . . . Hess, T. (2021). Strike-slip enables subduction initiation beneath a failed

842 rift: New seismic constraints from Puysegur Margin, New Zealand. *Tectonics*,

843 *40*(5), e2020TC006436. doi: https://doi.org/10.1029/2020TC006436

844 Smith, A., Hyndman, R., Cassidy, J., & Wang, K. (2003). Structure, seismicity,

845 and thermal regime of the Queen Charlotte transform margin. *Journal of*

846 *Geophysical Research: Solid Earth*, *108*(B11). doi: https://doi.org/10.1029/

847 2002JB002247

848 Spence, G., & Asudeh, I. (1993). Seismic velocity structure of the Queen Charlotte

849 basin beneath Hecate Strait. *Canadian Journal of Earth Sciences*, *30*(4), 787–

850 805. doi: https://doi.org/10.1139/e93-065

851 Stern, R. J., & Gerya, T. (2018). Subduction initiation in nature and models: A re-

852 view. *Tectonophysics*, *746*, 173–198. doi: https://doi.org/10.1016/j.tecto.2017

853 .10.014

854 Tian, Z., Freymueller, J. T., & Yang, Z. (2021). Postseismic deformation due to

855 the 2012 M w 7.8 Haida Gwaii and 2013 M w 7.5 Craig earthquakes and its

856 implications for regional rheological structure. *Journal of Geophysical Re-*

857 *search: Solid Earth*, *126*(2), e2020JB020197. doi: https://doi.org/10.1029/

858 2020JB020197

859 Tong, X., Sandwell, D. T., & Fialko, Y. (2010). Coseismic slip model of the 2008

860 Wenchuan earthquake derived from joint inversion of interferometric synthetic

aperture radar, GPS, and field data. *Journal of Geophysical Research: Solid Earth*, *115*(B4). doi: https://doi.org/10.1029/2009JB006625

Tréhu, A. M., Scheidhauer, M., Rohr, K. M., Tikoff, B., Walton, M. A., Gulick, S. P., & Roland, E. C. (2015). An abrupt transition in the mechanical response of the upper crust to transpression along the Queen Charlotte Fault. *Bulletin of the Seismological Society of America*, *105*(2B), 1114–1128. doi: https://doi.org/10.1785/0120140159

Waldhauser, F., & Ellsworth, W. L. (2000). A double-difference earthquake location algorithm: Method and application to the northern Hayward fault, California. *Bulletin of the seismological society of America*, *90*(6), 1353–1368. doi: https://doi.org/10.1785/0120000006

Wang, K., He, J., Schulzeck, F., Hyndman, R. D., & Riedel, M. (2015). Thermal condition of the 27 October 2012 M W 7.8 Haida Gwaii subduction earthquake at the obliquely convergent queen charlotte margin. *Bulletin of the Seismological Society of America*, *105*(2B), 1290–1300. doi: https://doi.org/10.1785/0120140183

Wei, S., Barbot, S., Graves, R., Lienkaemper, J. J., Wang, T., Hudnut, K., . . . Helmberger, D. (2015). The 2014 Mw 6.1 South Napa earthquake: A unilateral rupture with shallow asperity and rapid afterslip. *Seismological Research Letters*, *86*(2A), 344–354. doi: https://doi.org/10.1785/0220140249

Wetzler, N., Lay, T., Brodsky, E. E., & Kanamori, H. (2018). Systematic deficiency of aftershocks in areas of high coseismic slip for large subduction zone earthquakes. *Science advances*, *4*(2), eaao3225. doi: https://doi.org/10.1126/sciadv.aao3225

Zhang, H. (2003). *Double-difference seismic tomography method and its applications.* The University of Wisconsin-Madison.

Zhang, H., & Thurber, C. H. (2003). Double-difference tomography: The method and its application to the Hayward fault, California. *Bulletin of the Seismological Society of America*, *93*(5), 1875–1889. doi: https://doi.org/10.1785/0120020190

S